# Compact Traveling-Wave Physical Simulator for Human ESD

Leesa M. MacLeod, *Student Member, IEEE*, and Keith G. Balmain, *Life Fellow, IEEE*

***Abstract*— Existing travelling-wave electrostatic discharge (ESD) simulators satisfactorily reproduce the characteristics of a human discharge but have dimensions comparable to a human subject, so they are inconveniently large for practical ESD susceptibility testing of electronic equipment. This paper describes the design of a compact travelling-wave ESD simulator with benchtop-scale dimensions. The design process utilized frequency-domain measurements and computer simulations of wave attenuation on the part of the simulator representing the human arm. From these results, it was deduced that the ESD simulator arm could be shortened from its original human-scale length of 60 cm to a more compact 30 cm without significantly affecting the currents flowing on it. The part of the simulator representing the human body was designed on the basis of capacitance. The resulting travelling-wave simulator (arm and body) is approximately half the size of the original simulator. Measurements are presented comparing the compact simulator with a previously-designed full-size simulator and with a human test subject, with regard to arm currents, swept-frequency input impedance, and capacitance.**

## I. Introduction

SUSCEPTIBILITY of electronic equipment to human electrostatic discharge (ESD) can be tested by using an ESD simulator instead of a human subject. The ESD simulator must adequately reproduce the characteristics of a human discharge so that products being tested for ESD susceptibility are appropriately exercised. Presently, commercial ESD simulators are based on lumped-load resistor-capacitor circuits with a short metal discharge tip. At high frequencies the human arm and body act as a lossy distributed system over which the discharge wave propagates, a situation that cannot adequately be represented by lumped-load approximations [1]–[3]. In particular, a lumped-load simulator requires a ground strap which greatly distorts the near field [4] and can also affect the injected current, thus markedly influencing susceptibility measurements [5]. An ESD event can have a fast risetime, particularly for low voltage discharges [6]–[8]: thus, the ESD waveform includes high-frequency components, up to at least a few gigahertz. These high-frequency components affect susceptibility measurements in two ways: first, they can readily couple to circuit board traces, and second, high-speed circuits by their very nature tend to be particularly susceptible to high-frequency signals. It is therefore important that an ESD simulator correctly reproduce the high frequency components of a human ESD injected current (i.e., the first few nanoseconds of the ESD waveform) while at the same time making unnecessary the use of a ground strap that carries high currents and alters the near fields.

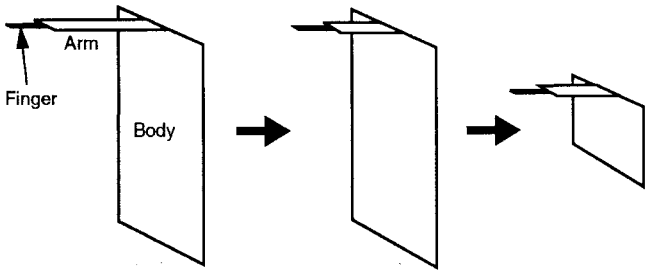


Fig. 1. ESD simulator compaction: (a) full-size, (b) shorten arm, and (c) shrink body.

A prototype travelling-wave ESD simulator (herein, referred to as the full-size simulator) has been designed (Balmain and Rayal [1]; Rayal [9]) to have properties similar to a human subject, as shown by comparative admittance measurements made at the fingertip. Note that the term "simulator" as used here excludes the arc discharge, thus representing the human hand, arm, and body, plus a finger or hand-held tool if required. This full-size simulator referred to above is about the same size as a person, and includes a finger as well as an arm and a body. The purpose of the present work is to analyze the currents flowing on the simulator and if possible reduce its size while retaining its ability to simulate a human discharge [10]. The greater portability and ease of positioning of a compact simulator would make it suitable for ESD tests on a wide range of products.

The discharge wave is expected to attenuate rapidly along the simulator arm, so the focus of the compaction process is on reducing the length of the simulator arm, as shown in Fig. 1. The width of the arm is held at 5 cm (the width of the full-size simulator arm). Since the finger region may be modified to simulate hand-metal conditions, as was done by Saini and Balmain [11], [12], this region is not dealt with here. With the arm reduced in length, the attached body panel is reduced in area so that the body capacitance remains the same as for the full-size simulator. In actual use, the simulator is charged through a high-value resistor ($\sim$100 M$\Omega$) attached at the lower

Manuscript received May 31, 1996; revised December 10, 1996. This work was supported by Bell Canada and the Natural Sciences and Engineering Research Council of Canada. This work was presented in part at the 1994 EuroEm International Symposium on Electromagnetic Environments and Consequences, Bordeaux, France.

The authors are with the Department of Electrical and Computer Engineering, University of Toronto, Toronto, Ont., Canada M5S 3G4 (email: macleod@waves.utoronto.ca).

Publisher Item Identifier S 0018-9375(97)03701-0.

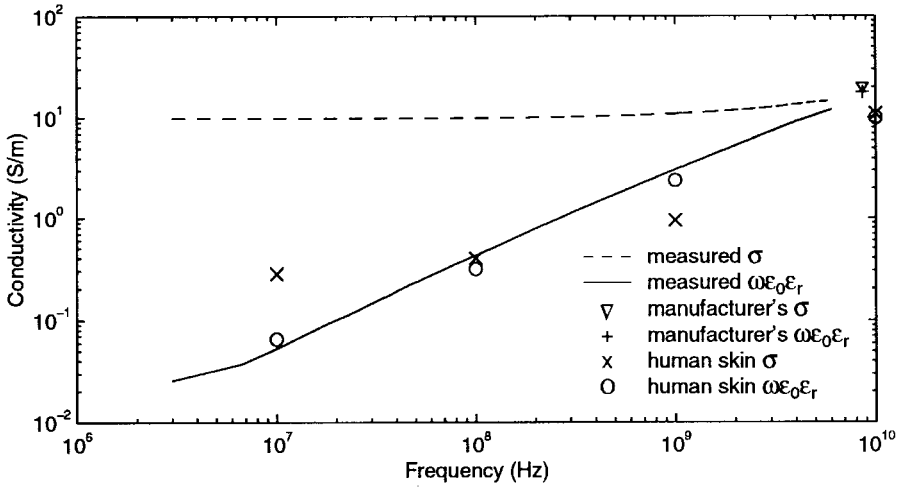


Fig. 2. Eccosorb VF and human skin properties [13], [14]. Measured quantities are derived from measured reflection coefficient.

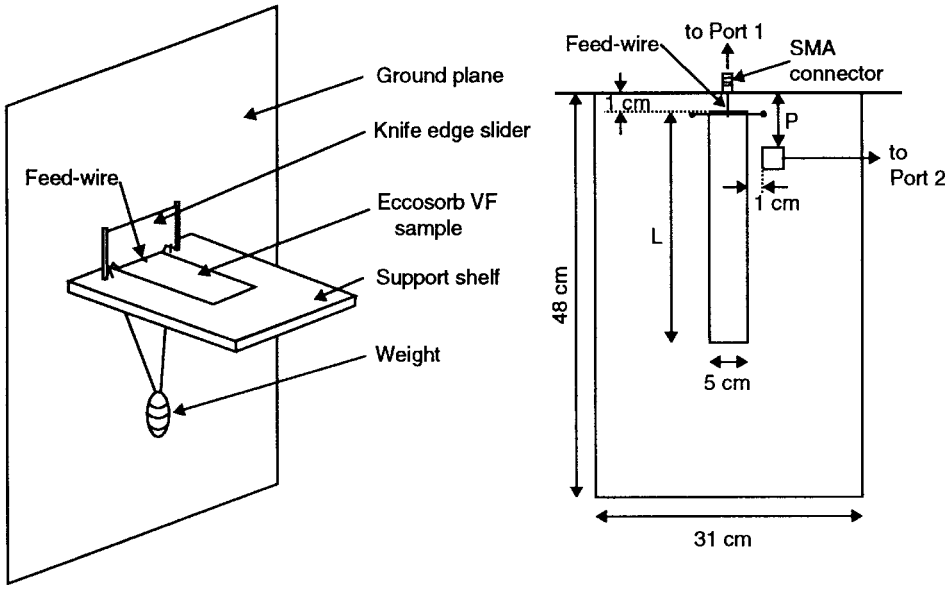


(a) (b)

Fig. 3. Measurement test fixture: (a) overall view and (b) details ($L$ = strip length, $P$ = position of loop probe).

extremity of the body panel. In contrast with the ground strap of a lumped-load ESD simulator, this attachment carries a negligible fraction of the discharge current and therefore has negligible effect on the discharge arc at the end of the "finger" and on the fields associated with the discharge.

## II. Material Properties

Eccosorb VF [13], a lossy dielectric material, takes the place of the human body in the ESD simulator. The conductivity $\sigma$ and the relative permittivity $\varepsilon_r$ of Eccosorb VF were determined in preparation for their use in a method-of-moments computer program. The swept-frequency complex reflection coefficient $\rho$ was measured by pressing an APC-7 connector against a thin sample of this material. A 0.26 mm thick VF-10 sample, rather than the 1.45 mm thick VF-60 used in the ESD simulator, was used to facilitate this simple $\sigma$ and $\varepsilon_r$ measurement technique. The APC-7 connector was connected to a vector network analyzer which measured the magnitude and phase of the reflection coefficient from 3 MHz to 6 GHz. The conductivity and relative permittivity curves derived from the measured reflection coefficient are shown in Fig. 2. The manufacturer-supplied material properties at 8.6 GHz are also shown in this figure, and follow the trend of the measured results. The conductivity and relative permittivity of human skin, as determined by Gabriel *et al.* [14], are also displayed in this figure. The permittivities of the two materials are in agreement, but the Eccosorb VF conductivity is higher than that of human skin.

## III. Description of Analysis Methods

### A. Measurements

A test fixture, shown in Fig. 3, was used to feed a signal to a VF-60 strip in a repeatable manner. It includes a large

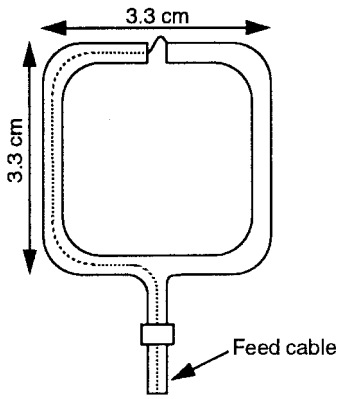


Fig. 4. Loop probe.

(91 cm by 118 cm) metal sheet acting as a ground plane, through which an SMA bulkhead connector is fed. The inner conductor (0.25 mm diameter) of this connector extends for 1.1 cm beyond the ground plane to form a feed-wire. A 31 cm by 48 cm cross-linked polystyrene (low-permittivity, low-loss) shelf is used to support a VF-60 strip. The VF-60 strip is positioned with one edge 1 cm from the ground plane and under the feed-wire. A dielectric "knife edge slider" weighted with a copper cylinder presses the feed-wire onto the VF-60 (the feed-wire overlaps the VF-60 strip by about 1 mm). Since the contact position and contact pressure on the strip are well defined, this provides a repeatable means of contacting the VF-60 strip.

A balanced loop probe (Fig. 4) was used to measure the fields near the VF-60 strip and thus get an indication of the currents flowing on it. The loop is constructed from $0.085''$ diameter semi-rigid coaxial cable. The loop lies in the same plane as the VF-60 strip, and its position is given by the distance $P$ between the ground plane and the closest edge of the probe (in the direction perpendicular to the ground plane). The distance from the edge of the VF-60 strip to the closest side of the probe is 1 cm.

In order to measure the VF-60 strip properties in the frequency domain, the SMA connector on the test fixture ground plane was attached to port 1 of an HP 8753C vector network analyzer and $S$-parameter test set. Port 2 of the network analyzer was attached to the probe. The probe was moved progressively farther away from the ground plane, parallel to the VF-60 strip, and the swept-frequency $S$-parameters were recorded at each probe position. The change in the probe signal as it is moved farther from the feed-wire indicates the attenuation of the currents on the VF-60 strip. Measurements were performed in a shielded semi-anechoic chamber to reduce the effects of external interference and reflections from nearby objects.

### *B. Computer Simulations*

The computer simulator used in this work was *MBCPF* (version 164), which is a multiradius bridge current formulation of the frequency-domain method-of-moments [15]. The MBCPF computer program takes as input a grid of thin wire segments which may be loaded with simple RLC circuits at each segment end. A three-dimensional (3-D) material is thus modeled as a loaded wire grid as described by Balmain *et al*. [16]. This can be reduced to a two-dimensional (2-D) model for the thin VF-60 strip under consideration here.

The finite conductivity and the relative permittivity of the VF-60 material are accounted for by loading the square grid of wires with a resistor-capacitor network. The wires forming the perimeter of the strip are loaded at each end with the parallel connection of $R$ and $C$, while the internal wires are loaded at each end with the parallel connection of $2C$ and $R/2$. The values of the resistance $R$ and the capacitance $C$ are calculated at each frequency as

$$R = \frac{1}{\sigma t} \tag{1}$$

$$C = (\varepsilon_r - 1)\varepsilon_0 t \tag{2}$$

from the corresponding conductivity $\sigma$, permittivity $\varepsilon$, and thickness $t$ of the material.

The radius of these wires is chosen to obey the "same surface area" rule of thumb described by Ludwig [17], which states that "the surface area of the wires parallel to one linear polarization should be made equal to the surface area of the solid surface being modeled." Thus, the wire radius $r$ is calculated as

$$r = \frac{A}{N \times \pi \times L} \tag{3}$$

where $A$ is the surface area to be modeled, $L$ is the length of an individual wire segment (all wires in the grid are the same length), and $N$ is the total number of wires making up the grid. Here the number of wires in each of the two directions is taken to be the same, so that all wires are of the same radius.

The grid size (wire-to-wire spacing) is typically chosen to be one tenth of a wavelength [9], [10] or smaller. Since the VF-60 material is thin (at most 17% of the wavelength in the material), the free space wavelength is used in the calculation of the grid size. In these simulations, part of the wire grid structure is close to the ground plane; thus the grid must be small with respect to the feed-wire length or the wire-grid model would represent a wire over ground rather than a conducting sheet. Based on results of computer simulations using various grid sizes, a grid size of 5/12 cm (4.2 mm), corresponding to 12 wire segments across the 5 cm width of the VF-60 strip, was chosen as the best trade-off between increased accuracy (finer grid) and shorter calculation time (coarser grid). The grid size is thus 8.4% of the minimum free space wavelength of 5 cm.

In order to match the computer simulation to the measurement set-up, a 1 V generator is located between the ground plane and the 1 cm long feed-wire. The other end of this feed-wire attaches to the VF-60 strip at the midpoint of the edge closest to the ground plane, as shown in Fig. 5. In the computer simulations, the ground plane is infinite in extent. The wire segments in the computational model are shown in Fig. 5 for a VF-60 strip 25 cm long. The loop probe is included in the simulations unless otherwise noted.

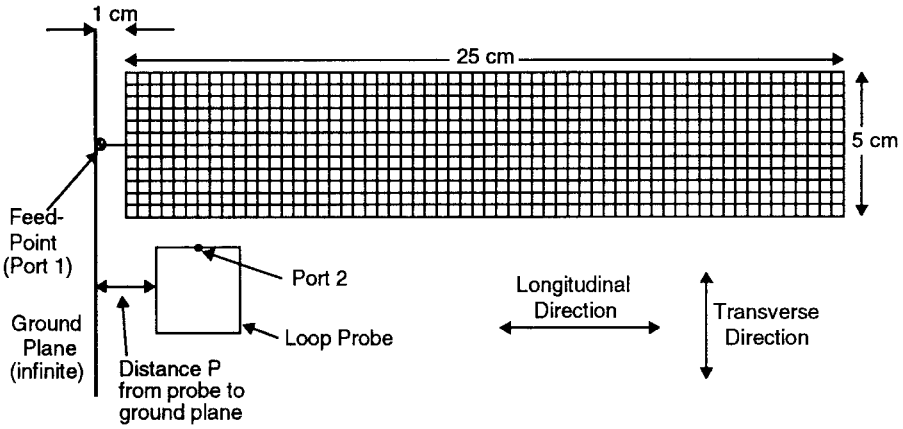


Fig. 5. Details of wire segments for computer simulator.

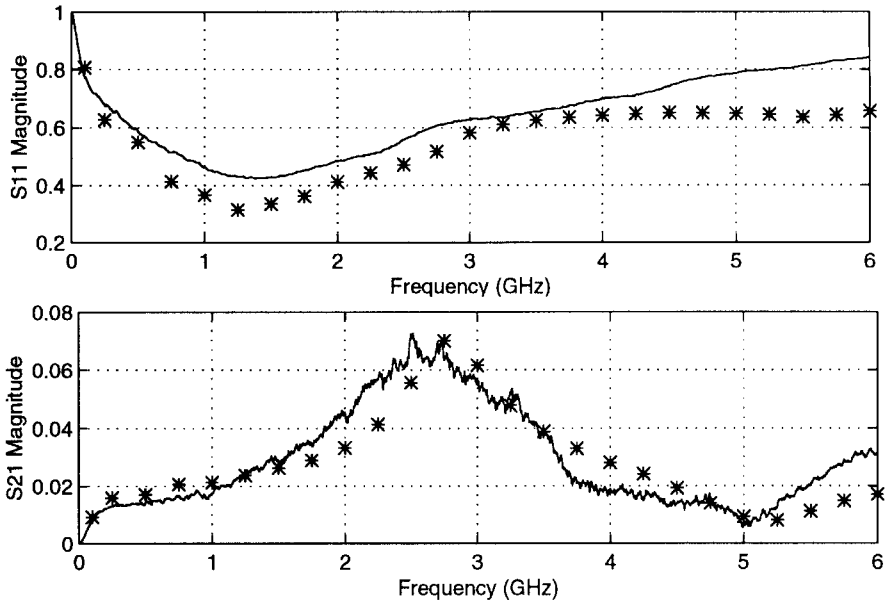


Fig. 6. Measured (solid line) and simulated (*) $S_{11}$ and $S_{21}$ (probe at 2 cm) for 25-cm long arm.

### C. Verification of Computer Simulation Results

Computer simulation results were compared with measurements in order to verify the accuracy of the currents calculated using MBCPF. The comparison was performed for a 5 cm by 25 cm VF-60 strip with the probe at various distances from the ground plane. The phase of the measured results is adjusted to account for a 7.5 mm difference in port 1 position and a 13.2 cm difference in port 2 position, between the computer simulations and the measurements (the distances are from the nearest connectors to the ports indicated in Fig. 5). Fig. 6 compares the measured and computer-simulated reflection coefficient magnitude and transmission coefficient magnitude, with the probe at 2 cm from the ground plane. The reflection coefficient simulations match the measurements, except in the 4–6 GHz range where the computer simulation underestimates by at most 22% the measured reflection from the strip. The transmission coefficient simulation results match the measurements when the probe is close to the ground plane, except for a deviation in the magnitude above 5 GHz. As the probe is moved farther away from the feed-point, the phase match deteriorates. Despite these small differences, the computer simulation results compare satisfactorily with measurements in the frequency range considered. Computer simulations can thus be used to study the currents on the VF-60 arm with confidence that these calculated currents are similar to those actually flowing on the arm of the physical simulator.

## IV. ESD Simulator Arm Truncation

### A. Current Maps

The MBCPF program calculates the complex current at each end of every wire segment in the simulation geometry. Thus several currents are associated with a junction of several wires (the wire grid consists of many wire junctions, as shown in Fig. 5). The currents are classified as those flowing in the wires parallel to the feed-wire (longitudinal direction) and those

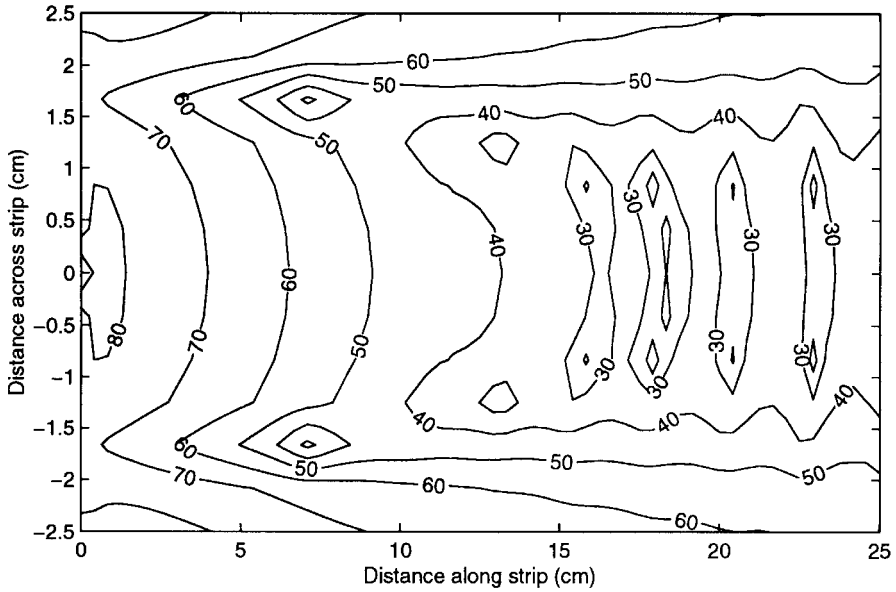


Fig. 7. Calculated longitudinal current magnitude at 6 GHz (contours at 10 dB increments with maximum current set to 100 dB).

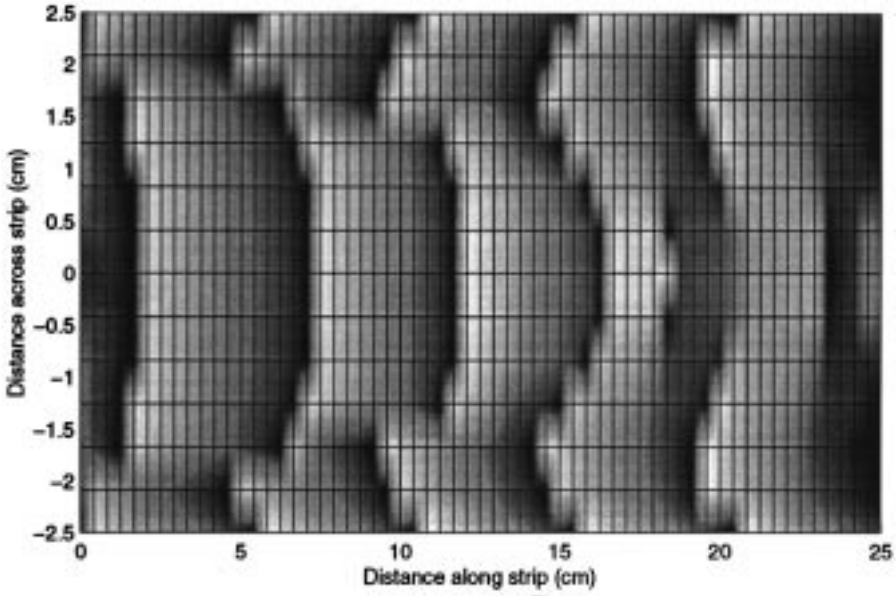


Fig. 8. Calculated longitudinal current phase at 6 GHz.

flowing perpendicular to the feed-wire (transverse direction). Here the longitudinal currents are considered; the current for plotting at each junction is that of the wire farthest from the feed-point.

The magnitude of the calculated currents on a 5 cm by 25 cm strip of VF-60 (with no probe present) at 6 GHz is shown in Fig. 7. The feed-wire attaches to the VF-60 strip at plot coordinates (0, 0). The current standing wave pattern due to reflections from the end of the strip is evident. The wavelength of this standing wave is about 4.48 cm, corresponding to a phase velocity of $2.69 \times 10^8$ m/s. Near the feed-point the current spreads out radially from the feed-point. Farther away from the feed-point the current is higher near the edges of the strip than at the center of the strip.

Fig. 8 shows the current phase in the longitudinal wires. The $-180°$ to $+180°$ transitions cause the abrupt black to white changes in these plots. By studying where these transitions (i.e., equiphase contours) occur, we see how the waves spread out from the feed-point. The phase transition spacing is about 4.48 cm, as expected from the wavelength evident in the standing waves of the magnitude plot. The direction of wave travel (perpendicular to the equiphase contours) on the center part of the strip is radially away from the feed-point, indicating the spread of spherical waves. In contrast, the phase at the edge of the strip indicates a wave progressing along the edge with a tilt toward the center region. This "edge effect" is also seen in the higher current magnitude near the edges of the strip. This indicates that the currents on the strip exist in two modes,

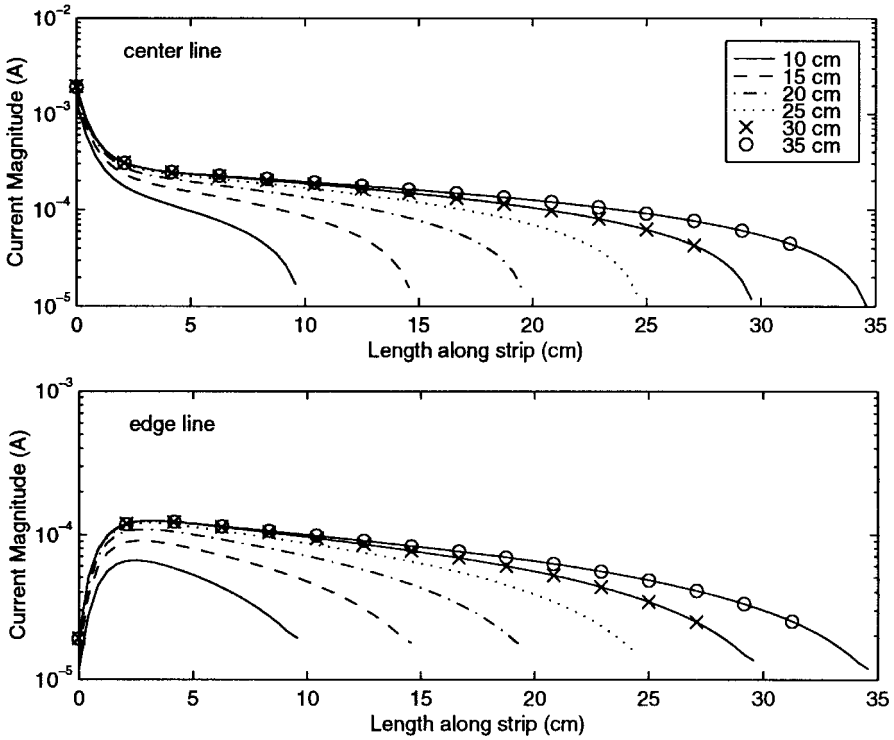


Fig. 9. Calculated longitudinal currents on strips (representing the arm) of length 10, 15, 20, 25, 30, and 35 cm plotted at the center and edge of each strip at 100 MHz.

one supported by the strip edge and the ground plane (space wave) and the other supported by the bulk of the strip itself (surface wave).

### *B. Determination of Truncation Point*

In the study of where the arm should be truncated, we are interested in the attenuation of the currents along the simulator arm. That is, if the currents have died out before they reach the end of the arm then the arm need not be so long. Thus, we focus on the magnitudes of the currents in the longitudinal wires. Since the longitudinal current magnitude plot is a surface or contour plot (as in Fig. 7), a comparison with currents on different length strips would be difficult to perform. Instead, we consider line plots of the longitudinal current magnitude along the center and the edge of each strip.

Simulations were run at 100 MHz, 250 MHz, 3 GHz, and 6 GHz on VF-60 strips of width 5 cm and lengths ranging from 10–35 cm (in 5 cm increments). These strips represent ESD simulator arms of various lengths. The currents on each length of strip are compared; when the currents match for increasing arm length, the length is no longer affecting the currents and thus the arm can be truncated. This comparison is carried out at each of the above frequencies.

The highest frequency of interest is 6 GHz, since this is the high frequency limit of the measurements and the simulation verification. At this frequency, all of the strips have very similar current characteristics from the feed-point to about 4 cm from the strip end. Most of the current flows on the edges of the strip. The reflection from the far end of the strip is apparent for each strip length (as in Fig. 7), but this reflection dies out quickly.

The lowest frequency of interest is 100 MHz; the free space wavelength at this frequency is 3 m, so for a structure of length about 30 cm ($\lambda/10$) or shorter the travelling-wave effect is not apparent (quasistatic situation). Fig. 9 shows the longitudinal current magnitude at the edge and at the center of the strips at 100 MHz. Here most of the current flows on the center region of the strip, rather than along the edges. The current on the shorter strips is significantly different from that on the longer strips; however, the two longest strips (30 and 35 cm) show similar characteristics.

These results indicate that the arm truncation point is constrained by the lower frequency (100 MHz) current distribution on the arm, since at higher frequencies the currents attenuate more rapidly. Since 30 cm is the length at which the 100 MHz current distribution does not change as the strip is lengthened further, we find that the arm can be cut at 30 cm without significantly affecting the currents flowing on it in the frequency range of interest.

### *C. Measurements to Confirm Truncation Point*

Two 5 cm wide strips of VF-60, one of length 32 cm and the other 62 cm, were constructed to verify by measurement that the arm can be truncated at 30 cm (the extra 2 cm is to facilitate attachment to the simulator body). Fig. 10 shows the reflection coefficient, which is very similar for the two arm lengths. Two-port measurements, also shown in Fig. 10 for the probe at 2 cm, indicate that the ESD simulator arm

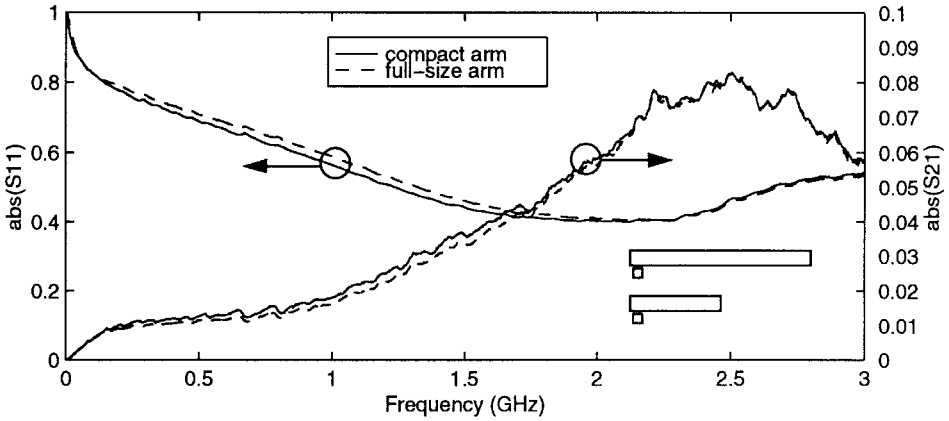


Fig. 10. Comparison of measured $S_{11}$ and $S_{21}$ with loop at 2 cm for full-size and compact arms. Inset shows the loop probe positions for the two arm lengths.

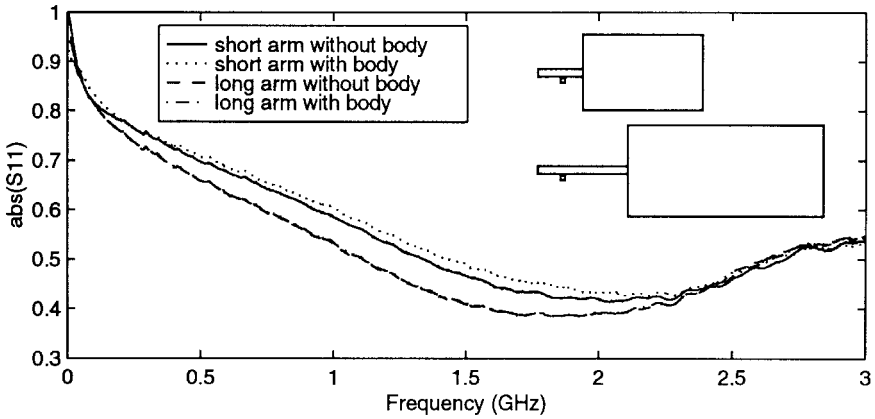


Fig. 11. Comparison of measured $S_{11}$ for long and short arms with and without body.

currents near the feed-point do not change appreciably due to the arm truncation.

## V. Complete Compact Simulator

### A. Body Size Calculation

The length of the compact simulator arm, as calculated in Section IV, is 30 cm. The corresponding size of the compact simulator body must now be determined. The capacitance of the body parallel to a ground plane, using a parallel plate approximation, is given by

$$C = \frac{\varepsilon_0 A}{d} \tag{4}$$

where $A$ is the body area and $d$ is the arm plus finger length. The area of the compact simulator body is chosen such that the above equation yields the same capacitance result for the compact simulator and the full size simulator. The full-size simulator body, corresponding to an arm plus finger length of 69 cm, is 60 cm by 130 cm. The body area requirement for the compact simulator, with an arm plus finger length of 39 cm, is thus 4400 cm$^2$, which is satisfied by using a 55 cm by 80 cm sheet of VF-60.

### B. Comparison of Full-Size and Compact Simulators and Effect of Adding Body to Simulator

For the compact simulator, tests were done to compare the input impedance and the currents with those of the full-size simulator. Measurements were also made to explore the effect of adding the body to the arm of the simulator. The test fixture is the same as that detailed in Section III-A. However, since the full-size simulator must also be accommodated by the test fixture, the fixture is elevated above the floor of the chamber.

A long arm and a short arm cut from the same sheet of VF-60 were found to be more similar, in terms of $S_{11}$ and $S_{21}$ measurements, than two short arms each cut from a different sheet of VF-60. This indicates that variations in the VF-60 material can mask the effect of changing arm length. This explains the results in [10], where differences between full-size and compact simulator characteristics were observed. In order to reduce the effect of material property variations, the arms used here were cut side-by-side from the same sheet of VF-60. Another possible source of error is the repositioning of the arm in the test fixture between measurements. This uncertainty was reduced, for measurements to determine the effect of adding the body, by first measuring the arm without the body, and then attaching the body to the arm (without adjusting the feed) and remeasuring.

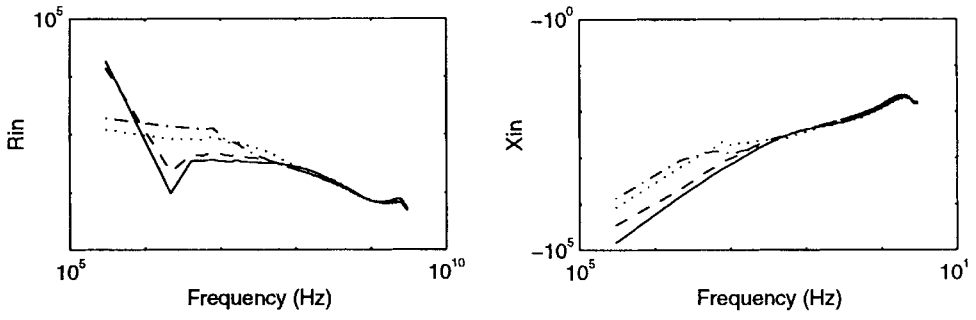


Fig. 12. Comparison of measured input impedance ($Z_{in} = R_{in} + jX_{in}$) for long and short arms with and without body (legend as in Fig. 11).

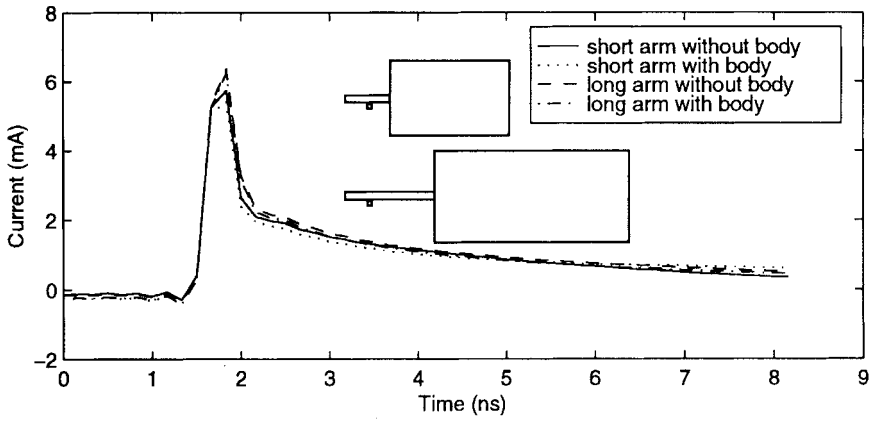


Fig. 13. Comparison of step responses of compact and full-size simulators.

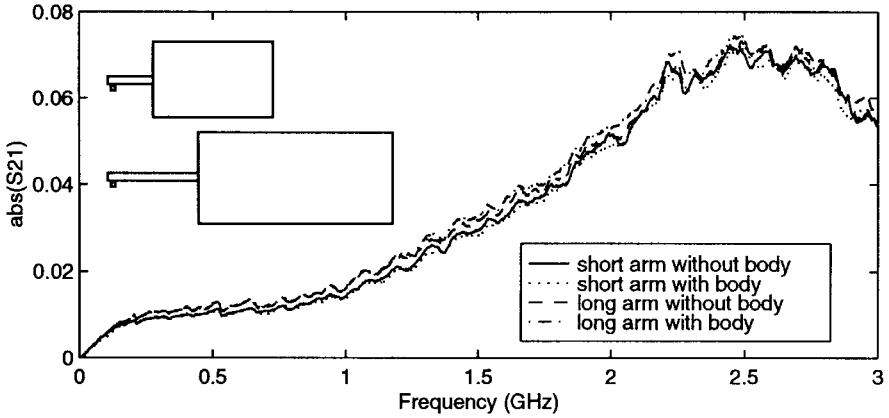


Fig. 14. Comparison of measured $S_{21}$ for compact arm with and without body; probe at 2 cm.

In Fig. 11, the reflection coefficients of the compact simulator and the full-size simulator with and without the body are shown. For both simulators, the effect of adding the body is only apparent when the results are transformed to input impedances, as shown in Fig. 12. At low frequencies, the effect of adding the body is apparent (the capacitance increases when the body is added). The data of Fig. 11 is also transformed into the time domain (using a fast Fourier transform (FFT) routine) to compare the step responses of the compact and full-size simulators (the step response can be thought of as the ESD discharge waveform when the arc is modeled as a perfect switch), as shown in Fig. 13. The compact simulator has the same step response as the full-size simulator for at least the first few nanoseconds of the waveform.

The two-port results are shown in Figs. 14 and 15 for the probe at positions 2 and 10 cm, respectively. The results indicate that the compact simulator is a good replacement for the full-size simulator.

### *D. Comparison of Compact Simulator With Human Subject*

The data from Rayal's work on the full-size simulator [9] is compared with the input admittance of the compact simulator and further measurements on the full-size simula-

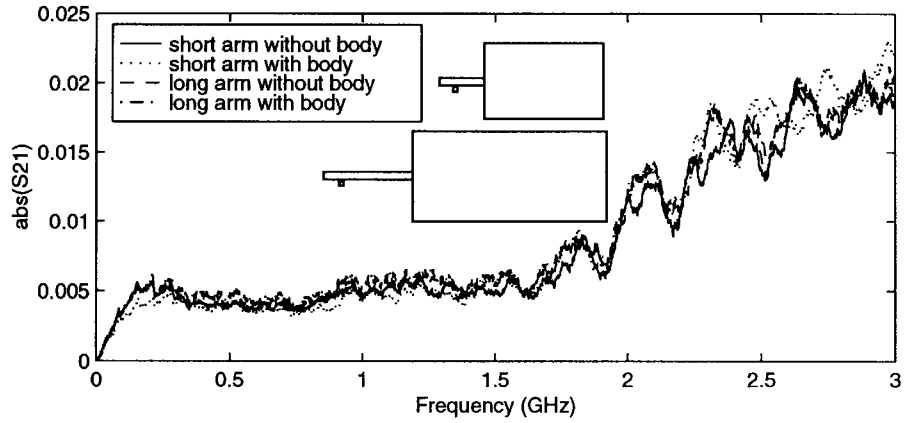


Fig. 15. Comparison of measured $S_{21}$ for compact arm with and without body; probe at 10 cm.

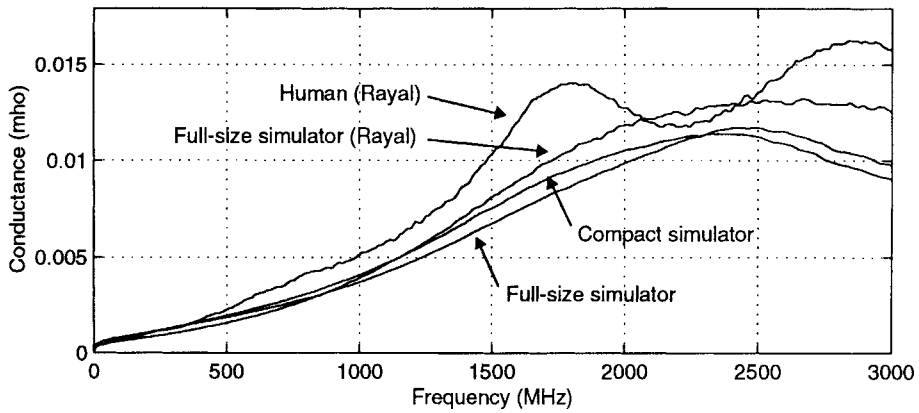


Fig. 16. Comparison of input conductance for a human subject and the full-size simulator from [9], and for the compact simulator and the full-size simulator (with finger) as measured here.

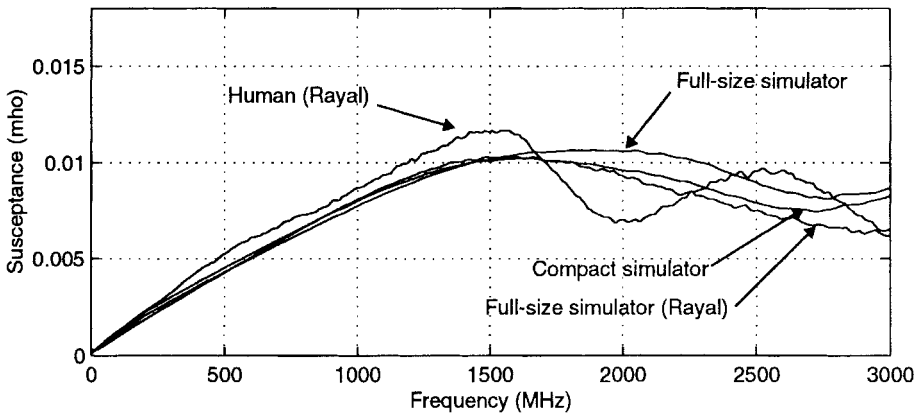


Fig. 17. Comparison of input susceptance for a human subject and the full-size simulator from [9], and for the compact simulator and the full-size simulator (with finger) as measured here.

tor. Both the compact simulator and the full-size simulator have a 2-cm wide, 9-cm long finger for these measurements. The comparison stops at 3 GHz as this is the limit of Rayal's measurements. The conductance comparison is shown in Fig. 16 and the susceptance comparison in Fig. 17. The two sets of full-size simulator curves are not identical because Rayal used a different measurement set-up than the one described here. These plots show that the compact and full-size simulators have properties near those of the human subject.

Capacitance measurements using a BK Precision Capacitance Meter indicate that the capacitance of the compact simulator over a ground plane is 55 pF compared with 61 pF for the full-size simulator and 56–78 pF for a human subject (depending on the distance and material between the subject's feet and the conductive floor). Extrapolation of the measured

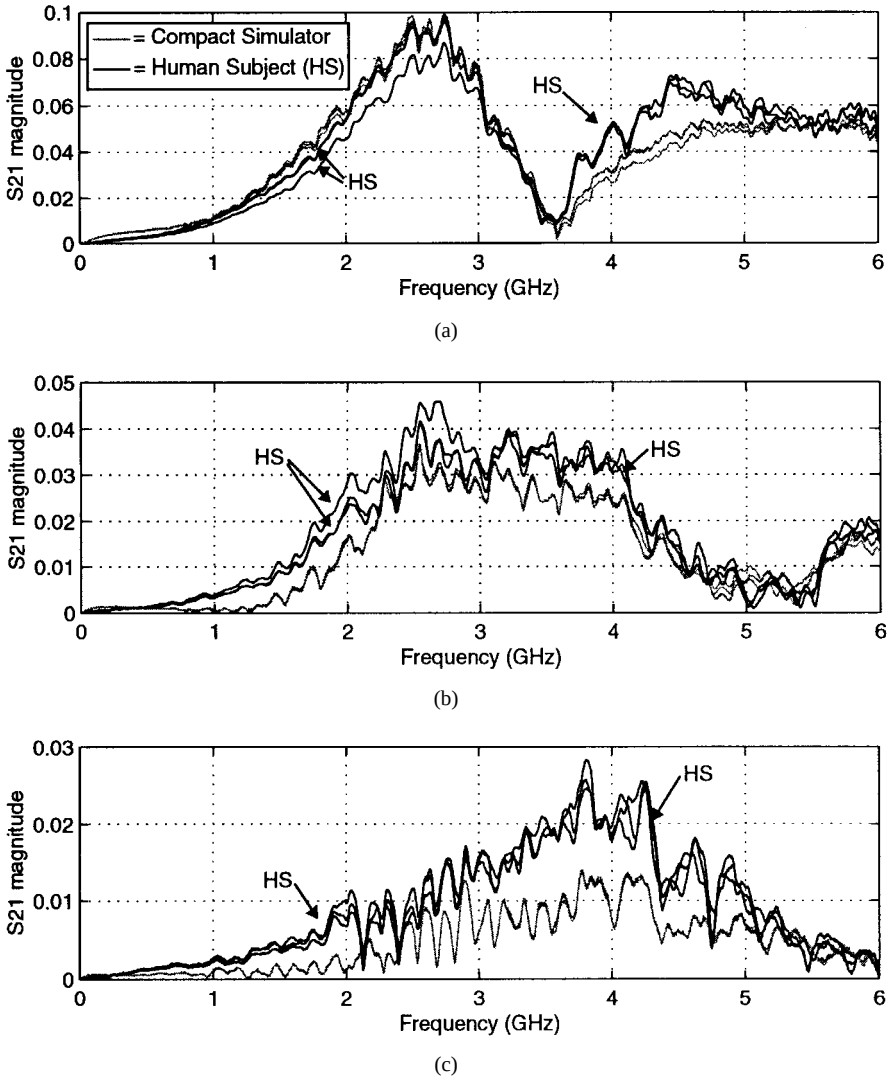


Fig. 18. Compact simulator compared with human subject: $S_{21}$ with loop at (a) 2 cm, (b) 10 cm, and (c) 25 cm. Three measurement trials are shown for each case.

reflection coefficient from Fig. 17 to zero frequency yields a capacitance of about 50 pF for the compact simulator and 64 pF for the full-size simulator.

Fig. 18 shows the transmission coefficients for the compact simulator and the human test subject, for the loop probe at 2, 10, and 25 cm, respectively. The measurements were performed using the test set-up of Fig. 3. For the human test subject measurements, the subject stood facing the ground plane with the extended arm palm-down on the support shelf and the tip of the middle finger pressed against the end of the feed-wire. Each measurement was performed three times to indicate measurement variability. The transmission coefficients for the human subject and the compact simulator match well when the probe is close to the feed-point. As the loop probe is moved farther from the ground plane, the transmission coefficient of (and thus the current flowing on) the compact simulator falls below that of the human test subject. This is consistent with the observation in [11] of greater attenuation in the travelling-wave simulator than in the human subject.

## VI. Conclusions

The full-size simulator has been reduced in size by a factor of two without significantly affecting its ability to simulate a human ESD event. This was determined by noting that the computer-simulated currents on a 30 cm VF-60 strip representing the ESD simulator arm are very close to those on the full-size 60 cm arm. Currents on arms shorter than 30 cm are considerably different than those on the 60 cm arm. Measurements comparing input impedance and currents on the 30 and 60 cm arms confirm that the 30 cm arm is a suitable replacement for the 60 cm arm and the human subject arm. A final set of measurements comparing the compact and full-size simulators (arms and bodies) confirms the validity of using a simple equivalent-capacitance formulation to find the size of the body to be attached to the compact simulator arm. The effect of variability in VF-60 properties was also noted and minimized for these measurements. The compact simulator adequately reproduces the response of the full-size simulator when the current delivered to the load and the fields close to

the discharge site are of prime concern, as is expected to be the case in the majority of testing situations. Measurements have been made of the wave attenuation along the arm of a human subject. These results indicate that the arm currents are similar to those on the travelling-wave simulators. Also, it is worth noting that the compact simulator does not require a ground strap, a feature which is the same as for the full-size simulator.

A computer simulation program based on the method of moments was found to be a useful design tool. The computer simulation results were validated by comparing them with measurements. The computer simulation program was then used to study the currents flowing on the ESD simulator arm. Thus fewer prototypes were required than if the design had been based on experimentation only. The computer simulation program also allowed study of the current distribution on the simulator arm, with regard to both standing and travelling waves.

## ACKNOWLEDGMENT

The authors would like to thank M. Cohen of Bell Canada.

## REFERENCES

[1] K. G. Balmain and F. Rayal, "Travelling-wave fast-transient ESD simulation," in *Proc. IEEE Int. Symp. Electromagn. Compat.,* Anaheim, CA, Aug. 17–21, 1992, pp. 455–459.
[2] R. K. Keenan and L. A. Rosi, "Some fundamental aspects of ESD testing," in *Proc. IEEE Int. Symp. Electromagn. Compat.,* Cherry Hill, NJ, Aug. 12–16, 1991, pp. 236–241.
[3] W. M. King, "Dynamic waveform characteristics of personnel electrostatic discharge," in *Proc. Electrical Overstress/Electrostatic Discharge Symp.,* Denver, CO, Sept. 24–27, 1979, pp. 78–87.
[4] D. Pommerenke and M. Aidam, "To what extent do contact-mode and indirect ESD test methods reproduce reality?" in *Proc. Electrical Overstress/Electrostatic Discharge Symp.,* Phoenix, AZ, Sept. 12–14, 1995, pp. 101–109.
[5] R. Wallace, "6 GHz time domain measurement of fast-transient events," in *Proc. IEEE Int. Symp. Electromag. Compat.,* Anaheim, CA, Aug. 17–21, 1992, pp. 460–463.
[6] A. S. Podgorski, J. Dunn, and R. Yeo, "Study of picosecond rise time in human-generated ESD," in *Proc. IEEE Int. Symp. Electromag. Compat.,* Cherry Hill, NJ, Aug. 12–16, 1991, pp. 263–264.
[7] B. Daout and H. Ryser, "The reproducibility of the rising slope in ESD testing," in *Proc. IEEE Int. Symp. Electromag. Compat.,* San Diego, CA, Sept. 16–18, 1986, pp. 467–474.
[8] ———, "Fast discharge mode in ESD-testing," in *Proc. 6th Int. Zurich Symp. Electromag. Compat.,* Zurich, Switzerland, Mar. 5–7, 1985, pp. 41–46.
[9] F. Rayal, "Travelling-wave electrostatic discharge simulation," M.A.Sc. thesis, Dept. Elect. Eng., Univ. Toronto, Toronto, Ont., Canada, 1992.
[10] L. M. MacLeod and K. G. Balmain, "Compact travelling-wave ESD simulator," in *Proc. Euro. Electromag. Int. Symp. Electromag. Environments and Consequences,* Bordeaux, France, May 30–June 3, 1994, pp. 1257–1264.
[11] R. Saini and K. G. Balmain, "Human hand/metal ESD and its physical simulation," in *Proc. Electrical Overstress/Electrostatic Discharge Symp.,* Phoenix, AZ, Sept. 12–14, 1995, pp. 90–94.
[12] ———, "Traveling-wave fast-transient human hand/metal ESD and its physical simulation, " *IEEE Trans. Electromag. Compat.,* to be published.
[13] Emerson and Cuming, "Eccosorb VF," Tech. Bull. 2–16, Sept. 1980.
[14] C. Gabriel, R. H. Bentall, and E. H. Grant, "Comparison of the dielectric properties of normal and wounded human skin material," *Bioelectromagnetics,* vol. 8, pp. 23–27, 1987.
[15] M. A. Tilston and K. G. Balmain, "A multiradius, reciprocal implementation of the thin-wire moment method," *IEEE Trans. Antennas Propagat.,* vol. 38, pp. 1636–1644, Oct. 1990.
[16] K. G. Balmain, C. C. Bantin, M. A. Tilston, A.-M. Chung, and T. D. Pham, "The moment method and extensions of wire-grid modeling for microwave heating," in *Proc. 28th Int. Microwave Power Institute Symp.,* Montreal, Canada, July 11–14, 1993, pp. 158–169.
[17] A. C. Ludwig, "Wire grid modeling of surfaces," *IEEE Trans. Antennas Propagat.,* vol. AP-35, pp. 1045–1048, Sept. 1987.

**Leesa M. MacLeod** (S'88) received the B.Sc. degree in electrical engineering from the University of New Brunswick, Fredericton, N.B., Canada, in 1992, the M.A.Sc. degree in electrical engineering from the University of Toronto, Toronto, Ont., Canada, in 1994, and is currently pursuing the Ph.D. degree in electrical engineering at the University of Toronto.

Her research area is the electromagnetic compatibility of digital circuits.

**Keith G. Balmain** (SM'85–F'87–LF'97) was born in London, Ont., Canada, on August 7, 1933. He received the B.A.Sc. degree in engineering physics from the University of Toronto in 1957, and the M.S. and Ph.D. degrees in electrical engineering, from the University of Illinois, Urbana, in 1959 and 1963, respectively.

He was an Assistant Professor of Electrical Engineering at the University of Illinois, associated primarily with the Aeronomy Laboratory, until 1966. He then joined what is now the Department of Electrical and Computer Engineering, University of Toronto, where he is a Professor and holder of the Bell Canada/NSERC Industrial Research Chair in Electromagnetics. He was Chairman of the Division of Engineering Science for two and a half years until 1987, after which he was Chairman of the University of Toronto's Research Board for a three-year term. His research has focused on antennas in plasma, broadband antennas, radio wave scattering from power lines and high-rise buildings, electrostatic charge accumulation and arc discharges on both spacecraft and human subjects, and electromagnetic compatibility. He coauthored the second edition of *Electromagnetic Waves and Radiating Systems*.

Dr. Balmain was co-recipient of the IEEE Antennas and Propagation Society Best Paper of the Year award in 1970, and in 1992 was co-recipient of a NASA Group Achievement Award, related to electrical grounding on the Space Station. He was on the IEEE Antenna Standards Committee and Chairman of the Subcommittee on Antennas in Physical Media from 1968 to 1976, Canadian chairman of the International Union of Radio Science Commission VI from 1970 to 1973, a member of the IEEE APS AdCom from 1973 to 1976, Associate Editor of *Radio Science* from 1978 to 1980, and Chairman of the Technical Program Committee, 1980 IEEE APS International Symposium.